Received: 16 January 2019 | Revised: 14 July 2019 | Accepted: 12 August 2019

DOI: 10.1002/asl.938

RESEARCH ARTICLE

Atmospheric Science Letters RMetS

Large-scale meteorological control on the spatial pattern of wintertime $PM_{2.5}$ pollution over China

Ziwei Wang[1] | Gang Chen[2] | Yu Gu[2,3,4] | Bin Zhao[2,3,5] | Qiao Ma[6] | Shuxiao Wang[7] | Kuo-Nan Liou[2,3]

[1]Department of Atmospheric and Oceanic Science, School of Physics, Peking University, Beijing, China

[2]Department of Atmospheric and Oceanic Sciences, University of California, Los Angeles, California

[3]Joint Institute for Regional Earth System Science and Engineering, University of California, Los Angeles, California

[4]University of California, Los Angeles Institute for Technology Advancement, Suzhou, China

[5]Pacific Northwest National Laboratory, Richland, Washington

[6]School of Energy and Power Engineering, Shandong University, Jinan, China

[7]School of Environment and State Key Joint Laboratory of Environment Simulation and Pollution Control, Tsinghua University, Beijing, China

Correspondence
Gang Chen and Yu Gu, Department of Atmospheric and Oceanic Sciences, University of California, Los Angeles, CA 90095.
Emails: gchenpu@atmos.ucla.edu (G.C.) and gu@atmos.ucla.edu (Y.G.)

Funding information
Division of Atmospheric and Geospace Sciences, Grant/Award Numbers: AGS-1608775, AGS-1701526, AGS-1742178; Natural Science Foundation of Jiangsu Province, Grant/Award Number: BK20171230

Abstract

The frequent episodes of severe air pollution over China during recent years have posed serious health threats to densely populated eastern China. Although several studies investigated the linkage between enhanced severity and frequency of air pollution and the large-scale weather patterns over China, the day-to-day covariability between them, as well as its local and remote mechanisms, has not been systematically documented. The wintertime synoptic covariability between $PM_{2.5}$ and large-scale meteorological fields is studied using surface observations of $PM_{2.5}$ in 2013/2014–2016/2017 and ERA-Interim meteorological fields through maximum covariance analysis (MCA). The first MCA mode (MCA1) suggests a consistent accumulation of ambient $PM_{2.5}$ as a result of weakened winds that block the pollutant removal passage in heavily polluted areas of eastern China, as well as moist air from southeast coast favoring haze formation. A northeast–southwest belt that extends into northeastern China and central China on each end is more sensitive to MCA1. The second MCA mode (MCA2) shows a north–south dipole in $PM_{2.5}$ linked to the contrast of boundary layer height and surface wind speed between northern and southern regions of China. Spatial patterns of both modes are supported by the GEOS-Chem chemistry transport model with realistic emission inventory. The spatial patterns of the two modes are robust on the interannual time scales. Based on that, we investigate the variability of the first two modes of the identified modes on the multidecadal scale by projecting GPM_500 pattern to 1981–2010. Correlation analysis of the projected time series and climate indices over 30 years indicates the possible linkage of Arctic oscillation, ENSO indices, Pacific decadal oscillation and east Atlantic/western Russia to regional air pollution patterns over China.

KEYWORDS

large-scale meteorology, $PM_{2.5}$ spatial patterns, synoptic control, teleconnection with climate indices

1 | INTRODUCTION

Severe air pollution episodes struck China quite frequently during recent years, posing serious threats to public health (Cohen *et al*., 2005; Silva *et al*., 2013; Geng *et al*., 2015; Wang *et al*., 2017). The key air pollutant of concern during the haze period is particulate matter (PM). Recent work showed that stagnant weather conditions and its persistency, besides other factors such as high emissions, secondary formation of PM and so forth, contributed substantially to the accumulation of fine PM (e.g., $PM_{2.5}$ with a diameter of 2.5 μm or less), deteriorating the visibility and thus affecting transportation and economic activity (Tao *et al*., 2014; Sun *et al*., 2017). These stagnant weather conditions tend to become more persistent under climate change, supported by multimodel ensembles (Horton *et al*., 2014).

With respect to the relationship between haze episodes and atmospheric circulation, previous studies focused on sensitivity of air pollution to regional scale meteorology (He *et al*., 2017; Megaritis *et al*., 2014). Zhao *et al*. (2013) also examined the vertical profile of particles, temperature and winds during a haze episode over the North China Plain on a local scale, demonstrating that heavy pollution might be caused by temperature inversion and weakened transport (Li *et al*., 2015). Most recently, Wang *et al*. (2018) suggested that 10-m wind speed as an index of horizontal dispersion and boundary layer height as an indicator of the strength of vertical mixing should be considered as the threshold of air stagnation conditions, indicating that these two variables should be examined when defining stagnant weather conditions.

From the perspective of large-scale meteorology, Zhang *et al*. (2016) showed that increased frequency of air pollution over Beijing and its neighboring region is associated with the shallowed east Asia trough and weak Siberian high. Leung *et al*. (2018) showed dominant synoptic weather parameters differ from one subregion to another, based on day-to-day variability. Some recent studies show that Arctic sea ice loss in the preceding autumn, which favors a reversed northeast–southwest pressure gradient that weakens the east Asian winter monsoon (EAWM) (Wang and Chen, 2016; Zou *et al*., 2017), might also contribute to intensified pollution episodes, although a large fraction of the observed trend can be attributed to atmospheric internal variability (Xue *et al*. 2017).

Although several studies have shed light on the linkage between enhanced severity and frequency of air pollution and the large-scale weather patterns (Chen *et al*., 2008; Niu *et al*., 2010), the day-to-day covariability between air pollution and large-scale meteorology fields over the entire China, as well as its local and remote mechanisms, have not been systematically documented. In this study, we apply maximum covariance analysis (MCA) to the covariance matrix of $PM_{2.5}$ and meteorological factors, and obtain leading modes of variability for the wintertime $PM_{2.5}$ and investigate the long-term large-scale meteorological controls over entire China. The observed patterns are further supported by the simulations from the GEOS-Chem chemistry transport model (CTM) with realistic emission inventory. We extend the time series of the MCA modes to the period of 1981–2010, and thus get the projected variability on the decadal time scale to further explore whether past climate variability plays a role in the stagnant weather conditions and hence the air pollution over China.

2 | DATA AND METHODOLOGY

We use the MCA to identify the leading modes of covariability between high concentration of $PM_{2.5}$ in China and stagnant meteorological conditions. We focus on the winter months when pollutants are most severe, and the analysis is conducted for DJF (December–February) from 2013/2014 to 2016/2017. Because the MCA method only requires a common temporal dimension of two fields, the meteorological fields we analyzed cover a larger domain, including entire east Asia, India and also southern part of Russia (10°–70°N, 70°–160°E), in order to capture the large-scale teleconnection pattern influencing air pollution in China. Details of MCA could be found in Appendix S1.

The $PM_{2.5}$ observational data are obtained from China National Environmental Monitoring Center (http://www.cnemc.cn/). We applied quality control and interpolation and get a subset of 364 stations with continuous record during winters from December 2013 to February 2017. Details could be found in Appendix S2.

Meteorological data are obtained from ERA-Interim (ERA-I) reanalysis data, available from https://www.ecmwf.int/. It has a spatial resolution of 0.75° × 0.75°, with a temporal resolution of 6 hr. The set of data includes sea level pressure (SLP), geopotential, zonal and meridional winds at 10 m, 850 hPa and 500 hPa. Twelve-hourly boundary layer height data is obtained from ERA-I.

$PM_{2.5}$ observation at Beijing time has been converted to UTC to match that of meteorological data. Both datasets have been averaged to daily mean before applying MCA, and 21-day running mean is removed. Daily mean records are used here because it is the time scale that captures synoptic weather events interaction with air pollution.

3 | RESULTS AND DISCUSSION

3.1 | Spatial patterns of $PM_{2.5}$ in China and large-scale meteorological control

In this section, we show MCA results using observational data (station record for $PM_{2.5}$, ERA-Interim reanalysis for

meteorology fields) over winters from 2013/2014 to 2016/2017. With a focus on large-scale synoptic meteorology, we select SLP and geopotential at 850 and 500 hPa (GPM_850 and GPM_500). We perform MCA for $PM_{2.5}$ with SLP, GPM_850 and GPM_500, separately. The $PM_{2.5}$ singular vectors of the three MCA analyses are nearly identical (i.e., correlation coefficient greater than 0.98) as well as their $PM_{2.5}$ time series, so we regressed MCA patterns of GPM_850 and GPM_500 based on that of $PM_{2.5}$ and SLP. Figure 1 shows the mean state and the leading spatial covariance patterns of $PM_{2.5}$ and large-scale meteorology. As shown in the first column of Figure 1, $PM_{2.5}$ mean concentration over four winters are relatively higher over northern part of China (to the north of 34°N). Relatively high SLP occurs over eastern China, Mongolia and southern Siberia. East Asian trough can be easily identified from GPM_500. Winter monsoon over east Asia is characterized by the geostrophic wind flowing through the trough, which is believed

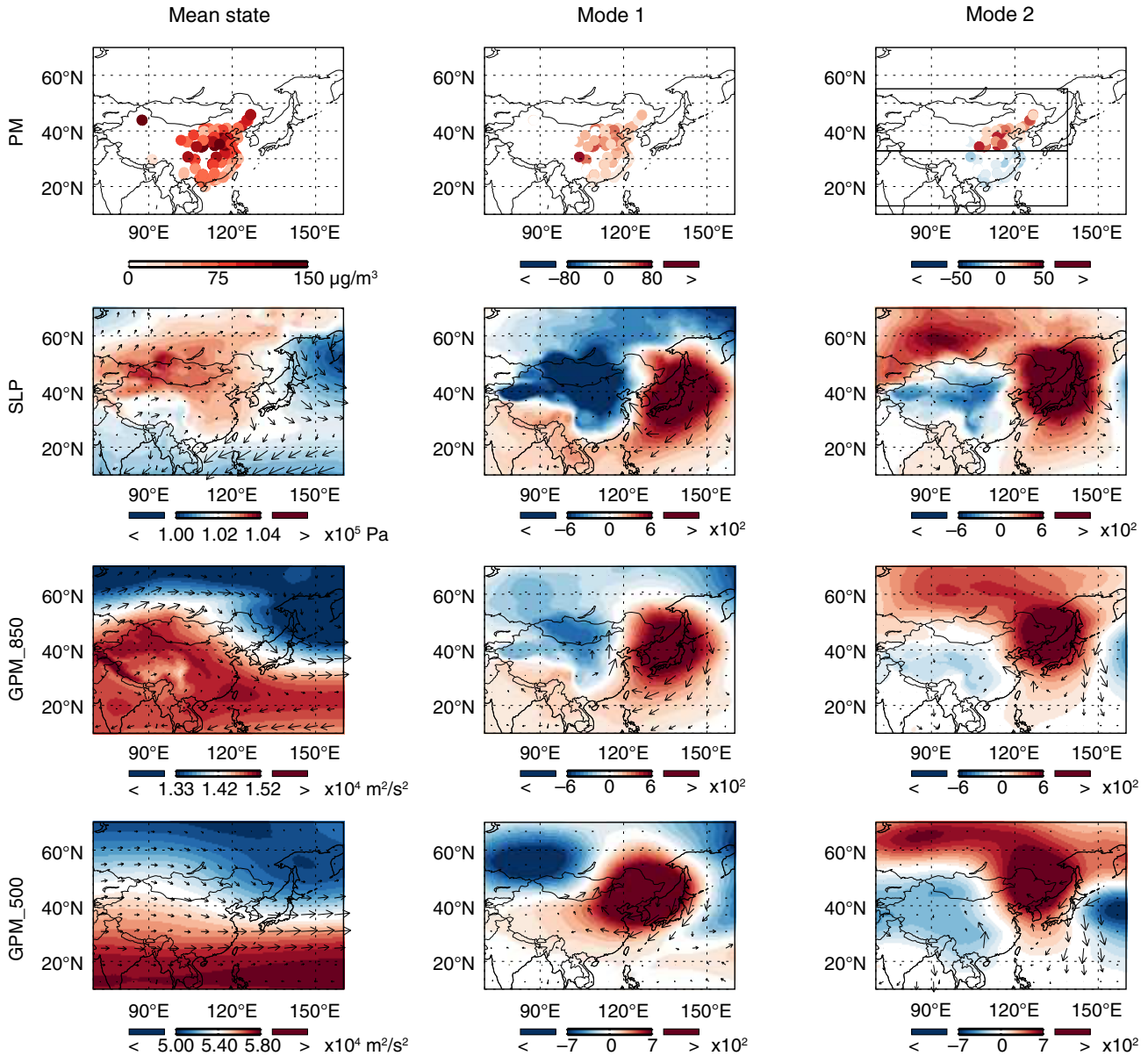

FIGURE 1 Spatial distributions of (left) time means and (middle) first and (right) second MCA modes of $PM_{2.5}$ and large-scale meteorology using data from 2013/2014 to 2016/2017. The singular vector patterns of MCA are scaled by the standard deviation of each time series to reflect their amplitudes. The variable of the singular vectors for each row from the top is $PM_{2.5}$, sea level pressure (SLP), and geopotential at 850 and 500 hPa, respectively. Horizontal winds of respective levels are plotted over shadings as vectors. Only stations (wind vectors over grids) that pass 90% significance test are shown. The two boxes in top-right subplot represents the northern (34°N–55°N, 70°E–140°E) and southern (15°N–34°N, 70°E–140°E) regions defined in this study

to be vital in transporting the pollutants toward tropics (Liu *et al*., 2003).

The first two modes combined explain 40–50% of the total squared covariance, and is assured that uncertainty does not compromise the particularity of each mode (Figure S1). Monte Carlo method is applied to test the significance of spatial regression patterns, please see Appendix S4 for details. In MCA1 (second column of Figure 1), the leading meteorological pattern resembles that reported by Cai *et al*. (2017) based on severe haze episodes in Beijing. Through the covariance of $PM_{2.5}$ and meteorological fields, it is found that the leading $PM_{2.5}$ patterns reflect a consistent accumulation of pollutant over the entire domain of China. The anomalous values reflect the sensitivity of ambient $PM_{2.5}$ concentration to meteorological parameters. More specifically, an area of higher concentration over Northern China Plain leads to a northeast–southwest belt that extends into northeastern China and central China on each end. At sea level, we see negative SLP anomaly over the high-pressure center, which may have led to weaker horizontal transport and comparatively weaker northerlies at the surface, resulting in the accumulation of pollutants over China. If we consider all three altitudes from surface to 500 hPa, it is obvious that there is a baroclinic structure of circulation anomaly tilting toward west, which is typical for synoptic weather systems. Such a structure contributed to the accumulation of air pollution by inducing a geostrophic southerly wind at 850 hPa near east coast and easterly wind with a southerly component near Yangtze River Delta at 500 hPa, by weakening northerlies and bringing warm and moist air to northern China (NC). In conclusion, at all altitudes, the winds induced by large-scale meteorological patterns weaken the climatological trough as shown in the mean state in Figure 1, which, in turn, blocks the transport of pollution through the passage. Furthermore, the southerly wind from coast brings humid air to polluted areas in NC, providing moisture for the formation of fog-haze events (Zhang *et al*., 2014).

In MCA2 (third column of Figure 1), a north–south dipole pattern exists for spatial distribution of $PM_{2.5}$, with positive values over the northern region (34°N–55°N, 70°E–140°E) of China and negative values over the southern region (15°N–34°N, 70°E–140°E). Corresponding meteorological fields (SLP and geopotential) all present a pattern with positive anomaly to the north of Japan and Siberia and a negative anomaly over central and western China. The contrast of $PM_{2.5}$ over northern and southern region of China can be explained by the anomalous northerly winds around 45°N at 850 hPa, indicating stronger intrusion of cold air from Siberia is able to reach NC. In particular, the region of cold air advection during the development of a typical mid-latitude cyclone is associated with anomalous sinking motion, thus creating stable conditions at boundary layer in northern region. Similar pattern has been proposed by Cheng *et al*. (2016), finding "north-higher south-lower" dipole pattern through composite analysis of stronger versus weaker winter monsoon years, which can be attributed to the difference of dry deposition.

We regressed surface wind speed and planetary boundary layer height back to the $PM_{2.5}$ time series, to see how horizontal and vertical dispersions contributed to the spatial distribution of $PM_{2.5}$. The regression patterns outside China are masked out to highlight the dispersion conditions over China. As shown in Figure S2, positive $PM_{2.5}$ values in northern region of China as shown in MCA1 are associated with anomalously low wind speed and boundary height, indicating stagnant weather conditions conducive to air pollution. Liu *et al*. (2013) also pointed out that weakened high-pressure center, which is accompanied by large-scale atmospheric movement, leads to subsiding airflow on local scale and suppressed PBL development. For MCA2, the southern region is dominated by relatively stronger surface wind and higher boundary layer height compared to northern region, partly explaining the relatively low values of $PM_{2.5}$.

In order to examine whether the patterns we found represent the actual pollution concentrations, domain averaged time series for northern and southern regions are calculated for comparison (black curves in Figure 2a,b). Gray stripes highlight the days when $PM_{2.5}$ concentration exceeds 150 $\mu g/m^3$, which is the standard of moderate pollution according to the regulation of air quality issued by Chinese government. The $PM_{2.5}$ time series of MCA1 (red curve in Figure 2a) captures the variation of both regions of China well, with correlation coefficients of 0.82 and 0.46 for northern and southern regions, respectively. For MCA2, the $PM_{2.5}$ time series is strongly correlated with $PM_{2.5}$ averaged over the northern region with a coefficient of 0.65, and negatively correlated with $PM_{2.5}$ over the southern region by −0.22, corresponding to the north–south contrast of the $PM_{2.5}$ singular vector pattern. This indicates the two MCA modes can work constructively to severe pollution episodes in NC and simultaneously destructively to pollution in southern China (SC).

For both modes, the time series of the three meteorological fields are well correlated (Figure 2c,d). This corroborates that the spatial structures of atmospheric circulation identified in Figure 1 are vertically coherent. Similar spatial structures can be recovered if the MCA is applied to $PM_{2.5}$ and a combined matrix of three meteorological fields.

3.2 | Model simulation

To confirm that the covariance patterns identified from observations are robust, we conducted model simulations

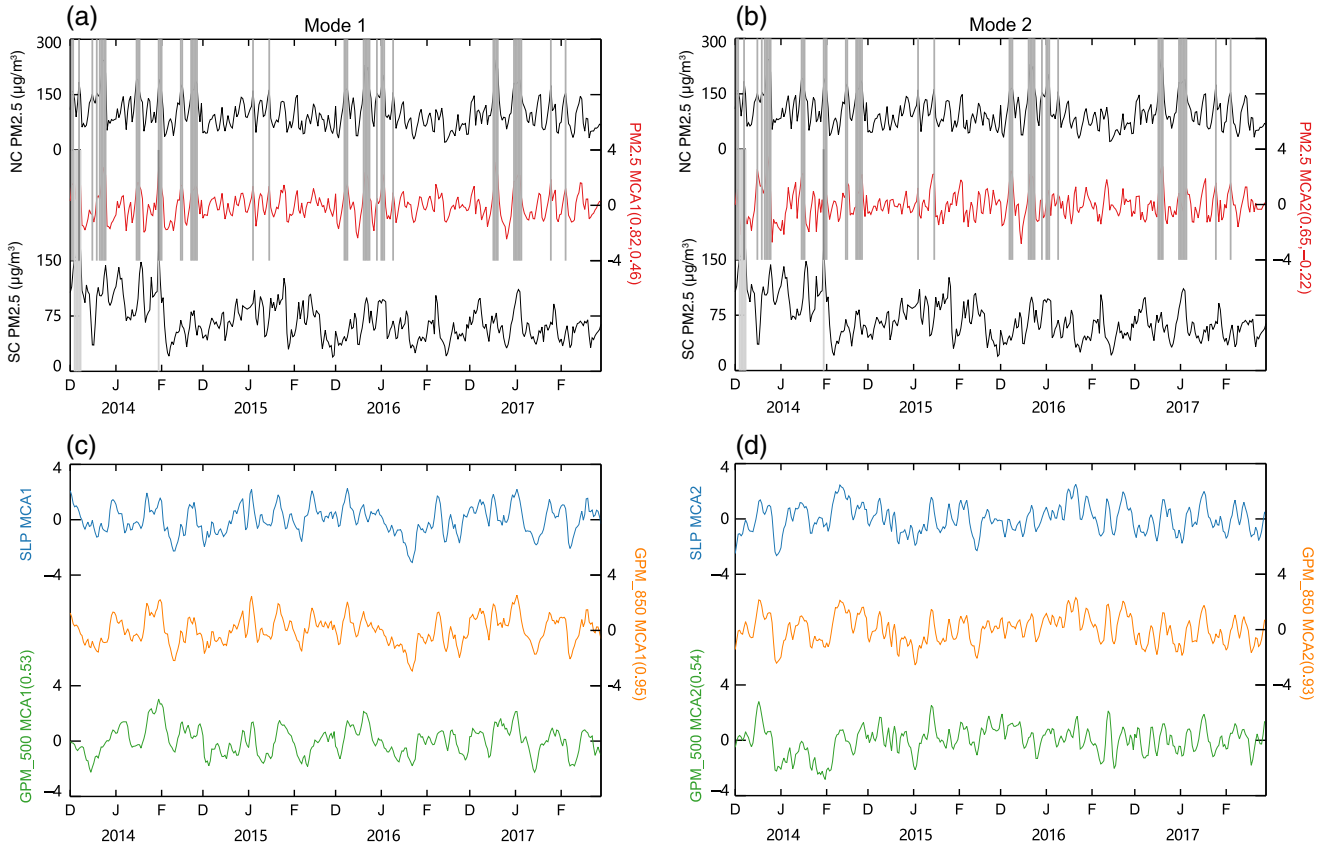

FIGURE 2 Time series of (left) first and (right) second MCA modes and the relation with domain averaged $PM_{2.5}$ in northern China (NC) and southern China (SC). In the top subplots are domain average time series of NC and SC in the first and third row, respectively, with the second row the normalized $PM_{2.5}$ time series for the covariability of $PM_{2.5}$ and SLP. Numbers in parentheses are correlation coefficients, with the former/latter one for NC/SC averaged time series. Gray stripes denote the days of which $PM_{2.5}$ concentration are over 150 μg/m^3, of which the darkest ones highlights the days for both NC and SC, the medium dark ones for NC only, and the lightest ones for SC only. In the bottom subplots are MCA time series of SLP, GPM_850 and GPM_500, respectively, with numbers in parentheses for correlation coefficients with SLP time series

using GEOS-Chem CTM v9-02, a regional CTM simulation using comprehensive chemistry processes and realistic emission inventory. Details of model setup could be found in Appendix S3.

In the analysis of the modeling results, we masked out simulated $PM_{2.5}$ concentrations for the grids outside mainland China, and used SLP, meridional and zonal winds at 10 m from the GEOS-5 reanalysis data that drive the model for the meteorological analysis. For grids above 90% confidence level, $PM_{2.5}$ grids are marked with "+", and only wind vectors over those grids are shown.

The mean state and MCA patterns of model simulation results match well with those obtained from observations (Figure 3). The $PM_{2.5}$ singular vector pattern of MCA1 retains positive and is associated with anomalous southerly wind, leading to accumulation of pollutants over the entire domain, especially over Northern China Plain. The $PM_{2.5}$ spatial pattern of MCA2 presents a dipole over the northern and southern regions, although the positive $PM_{2.5}$ values are confined in a narrower belt compared to observational results. Besides the similarity in spatial distributions, the amplitudes of both $PM_{2.5}$ and meteorological singular vector patterns are comparable to observational results shown in Figure 1.

It is noteworthy that the MCA patterns are similar even though only two winters of model simulations are analyzed. We have also divided observational dataset into first and latter 2-year periods, and performed the MCA for each group separately. We find that their spatial patterns (Figure S3) are relatively independent of the period examined. The weak dependence on the year of interest is consistent with the notion that the MCA modes represent the daily interactions between synoptic weather (e.g., east Asian trough) and pollution episodes. This gives us a sound basis to investigate the variability of patterns identified over a longer time scale, and to see if the stagnant patterns are potentially related to climate variabilities.

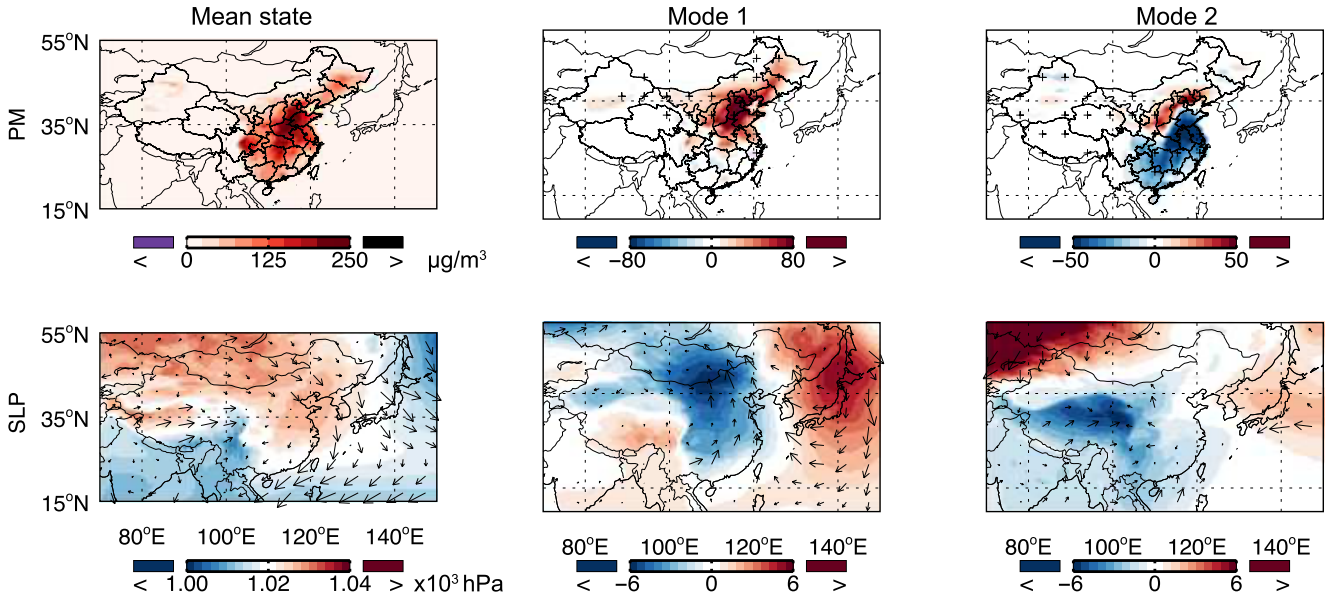

FIGURE 3 As in Figure 1, but for the model simulation results using GEOS-Chem with realistic emission inventory. $PM_{2.5}$ pollutants outside mainland China is masked out for the MCA modes, considering the meteorological control over mainland China merely. $PM_{2.5}$ grids above 90% confidence interval are marked with "+", and only wind vectors over grids that pass 90% significance test are shown. Surface winds (at 10 m level) are plotted over shadings as vectors. Note the model domain is slightly smaller than the reanalysis domain used in Figure 1

3.3 | Possible linkage between climate variability and stagnant weather conditions

We have also selected some climate indices to investigate whether the observed large-scale circulation patterns show significant correlation with any climate index influencing east Asia. Here we assume the MCA singular vectors of meteorology will hold beyond the 4 years we have examined due to its relatively weak dependence on the year examined, and thus we can extend the GPM_500 time series of each MCA mode by projecting the geopotential height over the period of 1980/1981–2009/2010 based on singular vectors. We choose Arctic oscillation (AO), ENSO indices (Nino1+2 and Nino3.4), Pacific decadal oscillation (PDO) and east Atlantic/western Russia (EA/WR) for our research, which are climate indices for mid- to high-latitudes of Northern Hemisphere (Table S1).

Table 1 shows the correlation of the extended GPM_500 time series with different climate indices. EA/WR is strongly correlated with MCA1 (with a correlation coefficient of 0.53), which makes sense as it almost synchronizes with EAWM and Siberian high (Lim and Kim, 2016). AO has a statistically significant positive correlation of 0.33 with MCA2. When AO is at a positive phase, the westerly component of jet stream around the Arctic Circle grows stronger, which in turn obstructs the cold polar air from striking toward mid-latitudes, weakening the east Asian trough and helping build up the patterns of MCA2 (Thompson and Wallace, 1998). This is supported by the recent work of Martineau *et al*. (2017), pointing out that the positive phase of AO is associated with reduced frequency in persistent cyclonic wave events over east Asia, significantly lessening the chance of reaching northern parts. For ENSO and PDO, we found a statistically significant negative correlation of −0.24 of Nino1+2 and −0.32 of PDO with MCA2. ENSO and PDO interact together and modify EAWM patterns by an obvious zonal shift of wind path, and turns out to be closely linked to temperature dipole patterns over eastern China, resulting in the contrast of stability of boundary layer and thus pollution dissipation (Zhu and Yang, 2003; Chen *et al*., 2013a; 2013b).

3.4 | Historical records of projection from 1981 to 2010

Based on previous results, we want to know whether intensity of preceding MCA patterns has substantially changed over several decades. We projected the MCA1 and MCA2

TABLE 1 Correlation coefficients of the extended DJF MCA1 and MCA2 time series for GPM_500 with different climate indices in 1980/1981–2009/2010

	AO	Nino1+2	Nino3.4	PDO	EA/WR
MCA1	0.16	0.14	0.12	−0.02	0.53[a]
MCA2	0.33[a]	−0.24[a]	−0.06	−0.32[a]	0.03

[a]For correlation coefficients passing two-tailed students' 10% test.

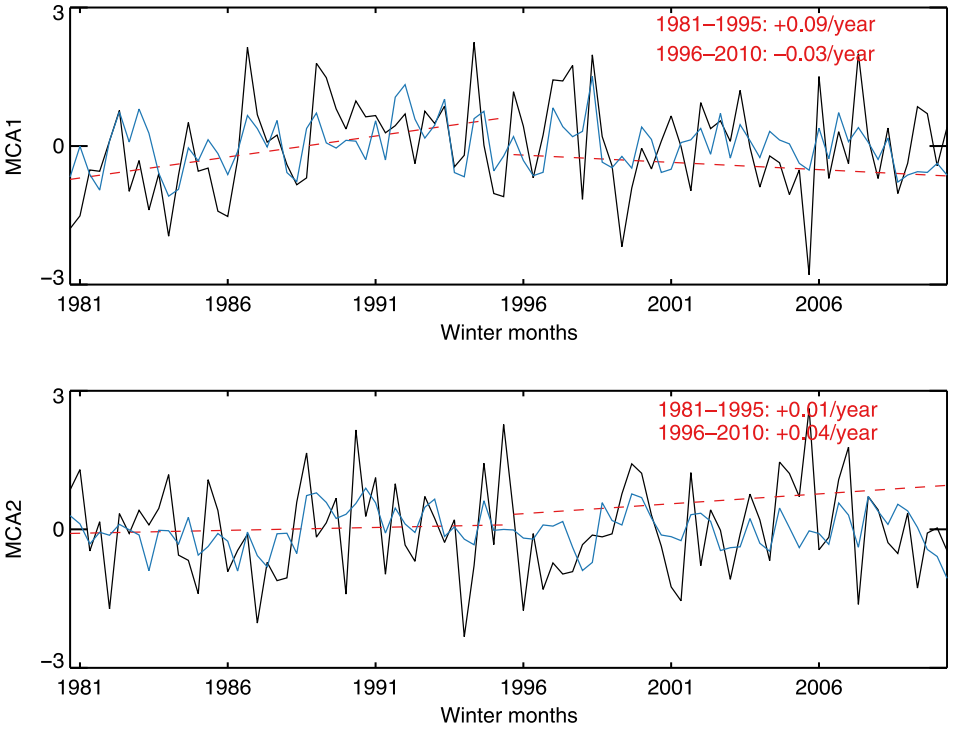

FIGURE 4 Monthly historical projections of MCA1 and MCA2 and their trend during 1981–1995 and 1996–2010, respectively. Solid black lines are temporal series of GPM_500 historical monthly record of MCA1 and MCA2 divided by standard deviation showing in panel (a) and (b), respectively. Dashed lines are correspondent linear regression results of 1981–1995 and 1996–2010, expressed in numerical form at the top-right corner. The slope calculated from monthly projection is multiplied by 3 months and translated to increase (or decrease) per year

spatial patterns toward historical monthly record of geopotential from wintertime of 1980/1981 to 2009/2010 at 500 hPa as illustrated by Equation (3) (projection, see Appendix S1), which reflects the intensity of such geopotential patterns. Linear regression for our pattern intensities are shown (Figure 4), and a modest increasing trend in projection is identified. The 30-year period is divided into the first period (1981–1995) and second period (1996–2010), to see if the modes behave differently over the two periods. All of the linear regressions passed two-tailed 10% Student's *t* test. We find a stronger increase in MCA1 during the first period, at 0.09 per year. Jiang and Tian (2013) suggested that EAWM tend to be strengthened compared with 1980–1999 period for areas to the north of 25°N, consistent with the upward trend of MCA1 during the first period. This contrast in dominant increasing time period between MCA1 and MCA2 suggests the trough-shallowing southerlies' contribution to the stagnant weather condition over eastern China was strongly enhanced during the first period, and a contrast of relatively higher concentration in the northern region enhanced slowly during the second period.

4 | CONCLUSIONS

In this study, we examined the spatial patterns of wintertime $PM_{2.5}$ over China and determined what patterns of large-scale meteorology field contributed to the accumulation (or removing) of $PM_{2.5}$ based on both observational data and model simulation results.

Using station observational $PM_{2.5}$ data and reanalysis meteorological fields from winters of 2013/2014 to 2016/2017, we have identified two important modes using MCA method. We successfully reproduced large-scale meteorology patterns proposed by Cai *et al*. (2017) in MCA1, in which the pattern-induced winds shallows the trough, weakening the northwesterly wind and building up a stagnant weather condition over eastern China. Beyond that, we showed that the spatial pattern of $PM_{2.5}$ is coherent over much of China due to the large-scale structure of synoptic weather systems. In MCA2, $PM_{2.5}$ presents a north–south dipole pattern with enhanced/reduced $PM_{2.5}$ concentrations in NC/SC. The contrast is caused by relatively stronger surface wind and higher boundary layer height in the southern region. Model simulations using GEOS-Chem with realistic emission inventory verified the robustness of these patterns, reproducing both pattern and amplitude identified in previous section.

We projected MCA patterns to extend DJF GPM_500 time series with different climate indices in 1980/1981–2009/2010, and investigate how the patterns correlate with climate indices. The historical record of geopotential time series shows high positive correlation with EA/WR for MCA1 only, highlighting the synchronization with Siberian high and strength of EAWM, while correlation with AO at MCA2 denotes cold air intrusion to NC. A statistically significant negative correlation with Nino1+2 and PDO also exists for MCA2, linked to temperature dipole

over eastern China and thus boundary layer stability. The differences in correlation imply different regional fingerprints of these climate indices, and the mechanisms for these relationships had been documented and supported by various papers.

The MCA modes identified in this study may be important for future research and air quality prediction. They connect the $PM_{2.5}$ pollution pattern with corresponding large-scale meteorological fields, manifesting that anomalies in high pressure at surface level over East China Sea and those in low pressure at 500 hPa over west Siberia play a role in controlling the pollution concentration over eastern China. It is worth investigating how future climate change would affect the intensity of the patterns, and how the patterns would respond to different representative concentration pathways (RCPs).

ACKNOWLEDGEMENTS

G.C. is supported by NSF awards AGS-1742178 and AGS-1608775. Y.G. and B.Z. are supported by the NSF AGS-1701526. Y.G. also acknowledges the support of the Natural Science Foundation of Jiangsu Province, China (No. BK20171230). We acknowledge the support of the Joint Institute for Regional Earth System Science and Engineering in the University of California Los Angeles. Z.W. acknowledges the computing resources at Peking University. All data needed to evaluate the conclusions are present in this article and/or the Supplementary Information. Additional data related to this paper can be requested from the authors.

CONFLICT OF INTEREST

The authors declare no conflict of interest.

ORCID

Ziwei Wang https://orcid.org/0000-0001-7813-4488

REFERENCES

Cai, W., Li, K., Liao, H., Wang, H. and Wu, L. (2017) Weather conditions conducive to Beijing severe haze more frequent under climate change. *Nature Climate Change*, 7, 257–262. https://doi.org/10.1038/nclimate3249

Chen, W., Feng, J. and Wu, R.G. (2013a) Roles of ENSO and PDO in the link of the east Asian winter monsoon to the following summer monsoon. *Journal of Climate*, 26, 622–635. https://doi.org/10.1175/JCLI-D-12-00021.1

Chen, W., Wei, K., Wang, L. and Ma, Y. (2013b) Climate variability and mechanisms of the east Asian winter monsoon and the impact from the stratosphere. *Chinese Journal of Atmospheric Sciences*, 37, 425–438. [in Chinese. https://doi.org/10.3878/j.issn.1006-9895.2012.12309

Chen, Z.H., Cheng, S.Y., Li, J.B., Guo, X.R., Wang, W.H. and Chen, D.S. (2008) Relationship between atmospheric pollution processes and synoptic pressure patterns in northern China. *Atmospheric Environment*, 42(24), 6078–6087. https://doi.org/10.1016/j.atmosenv.2008.03.043

Cheng, X., Zhao, T., Gong, S., Xu, X., Han, Y., Yin, Y., Tang, L., He, H. and He, J. (2016) Implications of east Asian summer and winter monsoons for interannual aerosol variations over central-eastern China. *Atmospheric Environment*, 129, 218–228. https://doi.org/10.1016/j.atmosenv.2016.01.037

Cohen, A.J., Anderson, H.R., Ostro, B., Pandey, K.D., Krzyzanowski, M., Künzli, N., Gutschmidt, K., Pope, A., Romieu, I., Samet, J.M. and Smith, K. (2005) The global burden of disease due to outdoor air pollution. *Journal of Toxicology and Environmental Health. Part A*, 68(13–14), 1301–1307. https://doi.org/10.1080/15287390590936166

Geng, G., Zhang, Q., Martin, R.V., van Donkelaar, A., Huo, H., Che, H., Lin, J. and He, K. (2015) Estimating long-term $PM_{2.5}$ concentrations in China using satellite-based aerosol optical depth and a chemical transport model. *Remote sensing of Environment*, 166, 262–270. https://doi.org/10.1016/j.rse.2015.05.016

He, J., Gong, S., Yu, Y., Yu, L., Wu, L., Mao, H., Song, C., Zhao, S., Liu, H., Li, X. and Li, R. (2017) Air pollution characteristics and their relation to meteorological conditions during 2014–2015 in major Chinese cities. *Environmental Pollution*, 223, 484–496. https://doi.org/10.1016/j.envpol.2017.01.050

Horton, D.E., Skinner, C.B., Singh, D. and Diffenbaugh, N.S. (2014) Occurrence and persistence of future atmospheric stagnation events. *Nature Climate Change*, 4(8), 698–703. https://doi.org/10.1038/nclimate2272

Jiang, D.B. and Tian, Z.P. (2013) East Asian monsoon change for the 21st century: results of CMIP3 and CMIP5 models. *Chinese Science Bulletin*, 58, 1427–1435. https://doi.org/10.1007/s11434-012-5533-0

Leung, D.M., Tai, A.P.K., Mickley, L.J., Moch, J.M., van Donkelaar, A., Shen, L. and Martin, R.V. (2018) Synoptic meteorological modes of variability for fine particulate matter (PM2.5) air quality in major metropolitan regions of China. *Atmospheric Chemistry and Physics*, 18, 6733–6748. https://doi.org/10.5194/acp-18-6733-2018

Li, J., Chen, H.B., Li, Z.Q., Wang, C.P., Cribb, M. and Fan, X.H. (2015) Low-level temperature inversions and their effect on aerosol condensation nuclei concentrations under different large-scale synoptic circulations. *Advances in Atmospheric Sciences*, 32(7), 898–908. https://doi.org/10.1007/s00376-014-4150-z

Lim, Y.K. and Kim, H.D. (2016) Comparison of the impact of the Arctic oscillation and Eurasian teleconnection on interannual variation in east Asian winter temperatures and monsoon. *Theoretical and Applied Climatology*, 124(1–2), 267–279. https://doi.org/10.1007/s00704-015-1418-x

Liu, H., Jacob, D.J., Bey, I., Yantosca, R.M., Duncan, B.N. and Sachse, G.W. (2003) Transport pathways for Asian pollution outflow over the Pacific: interannual and seasonal variations. *Journal of Geophysical Research*, 108(D20), 8786. https://doi.org/10.1029/2002JD003102

Liu, X.G., Li, J., Qu, Y., Han, T., Hou, L., Gu, J., Chen, C., Yang, Y., Liu, X., Yang, T., Zhang, Y., Tian, H. and Hu, M. (2013) Formation and evolution mechanism of regional haze: a case study in the megacity Beijing, China. *Atmospheric Chemistry and Physics*, 13(9), 4501–4514. https://doi.org/10.5194/acp-13-4501-2013

Martineau, P., Chen, G. and Burrows, D.A. (2017) Wave events: climatology, trends, and relationship to northern hemisphere winter blocking and weather extremes. *Journal of Climate*, 30(15), 5675–5697. https://doi.org/10.1175/JCLI-D-16-0692.1

Megaritis, A.G., Fountoukis, C., Charalampidis, P.E., Denier van der Gon, H.A.C., Pilinis, C. and Pandis, S.N. (2014) Linking climate and air quality over Europe: effects of meteorology on $PM_{2.5}$ concentrations. *Atmospheric Chemistry and Physics*, 14(18), 10283–10298. https://doi.org/10.5194/acp-14-10283-2014

Niu, F., Li, Z., Li, C., Lee, K.-H. and Wang, M. (2010) Increase of wintertime fog in China: potential impacts of weakening of the eastern Asian monsoon circulation and increasing aerosol loading. *Journal of Geophysical Research*, 115, D00K20. https://doi.org/10.1029/2009JD013484

Silva, R.A., West, J.J., Zhang, Y., Anenberg, S.C., Lamarque, J.F., Shindell, D.T., Collins, W.J., Dalsoren, S., Faluvegi, G., Folberth, G., Horowitz, L.W., Nagashima, T., Naik, V., Rumbold, S., Skeie, R., Sudo, K., Takemura, T., Bergmann, D., Cameron-Smith, P., Cionni, I., Doherty, R.M., Eyring, V., Josse, B., MacKenzie, I.A., Plummer, D., Righi, M., Stevenson, D. S., Strode, S., Szopa, S. and Zeng, G. (2013) Global premature mortality due to anthropogenic outdoor air pollution and the contribution of past climate change. *Environmental Research Letters*, 8 (3), 034005. https://doi.org/10.1088/1748-9326/8/3/034005

Sun, W., Hess, P. and Liu, C. (2017) The impact of meteorological persistence on the distribution and extremes of ozone. *Geophysical Research Letters*, 44, 1545–1553. https://doi.org/10.1002/2016GL071731

Tao, M., Chen, L., Xiong, X., Zhang, M., Ma, P., Tao, J. and Wang, Z. (2014) Formation process of the widespread extreme haze pollution over northern China in January 2013: implications for regional air quality and climate. *Atmospheric Environment*, 98, 417–425. https://doi.org/10.1016/j.atmosenv.2014.09.026

Thompson, D.W. and Wallace, J.M. (1998) The Arctic oscillation signature in the wintertime geopotential height and temperature fields. *Geophysical Research Letters*, 25(9), 1297–1300. https://doi.org/10.1029/98GL00950

Wang, H.-J. and Chen, H.-P. (2016) Understanding the recent trend of haze pollution in eastern China: roles of climate change. *Atmospheric Chemistry and Physics*, 16, 4205–4211. https://doi.org/10.5194/acp-16-4205-2016

Wang, J., Zhao, B., Wang, S., Yang, F., Xing, J., Morawska, L., Ding, A., Kulmala, M., Kerminen, V.-M., Kujansuu, J., Wang, Z., Ding, D., Zhang, X., Wang, H., Tian, M., Petäjä, T., Jiang, J. and Hao, J. (2017) Particulate matter pollution over China and the effects of control policies. *Science of the Total Environment*, 584–585, 426–447. https://doi.org/10.1016/j.scitotenv.2017.01.027

Wang, X., Dickinson, R., Su, L., Zhou, C. and Wang, K. (2018) $PM_{2.5}$ pollution in China and how it has been exacerbated by terrain and meteorological conditions. *BAMS*, 105–119, 105–119. https://doi.org/10.1175/BAMS-D-16-0301.1

Xue, D., Lu, J., Sun, L., Chen, G. and Zhang, Y. (2017) Local increase of anticyclonic wave activity over northern Eurasia under amplified Arctic warming. *Geophysical Research Letters*, 44(7), 3299–3308. https://doi.org/10.1002/2017GL072649

Zhang, R.H., Li, Q. and Zhang, R.N. (2014) Meteorological conditions for the persistent severe fog and haze event over eastern China in January 2013. *Science China: Earth Sciences*, 57, 26–35. https://doi.org/10.1007/s11430-013-4774-3

Zhang, Y., Ding, A., Mao, H., Nie, W., Zhou, D., Liu, L., Huang, X. and Fu, C. (2016) Impact of synoptic weather patterns and interdecadal climate variability on air quality in the North China Plain during 1980–2013. *Atmospheric Environment*, 124, 119–128. https://doi.org/10.1016/j.atmosenv.2015.05.063

Zhao, X., Zhao, P., Xu, J., Meng, W., Pu, W., Dong, F., He, D. and Shi, Q. (2013) Analysis of a winter regional haze event and its formation mechanism in the north China plain. *Atmospheric Chemistry and Physics*, 13(11), 5685–5696. https://doi.org/10.5194/acp-13-5685-2013

Zhu, Y. and Yang, X. (2003) Relationships between Pacific decadal oscillation (PDO) and climate variabilities in China. *Acta Meteorological Sinica*, 61, 641–654. [in Chinese. https://doi.org/10.11676/qxxb2003.065

Zou, Y., Wang, Y., Zhang, Y. and Koo, J.H. (2017) Arctic sea ice, Eurasia snow, and extreme winter haze in China. *Science Advances*, 3 (3), e1602751. https://doi.org/10.1126/sciadv.1602751

SUPPORTING INFORMATION

Additional supporting information may be found online in the Supporting Information section at the end of this article.

How to cite this article: Wang Z, Chen G, Gu Y, *et al.* Large-scale meteorological control on the spatial pattern of wintertime $PM_{2.5}$ pollution over China. *Atmos Sci Lett*. 2019;e938. https://doi.org/10.1002/asl.938